Pergamon

Atmospheric Environment Vol. 29, No. 18, pp. 2417–2427, 1995
Elsevier Science Ltd
Printed in Great Britain
1352-2310/95 $9.50 + 0.00

1352-2310(95)00190-5

LAGRANGIAN STATISTICS IN TURBULENT CHANNEL FLOW

QUNZHEN WANG, KYLE D. SQUIRES and XIAOHUA WU

Department of Mechanical Engineering, Votey Building, University of Vermont, Burlington, VT 05405, U.S.A.

(*First received* 5 *January* 1995 *and in final form* 4 *April* 1995)

Abstract—Lagrangian statistics have been obtained from large eddy simulations of fully developed turbulent channel flow. Calculations were performed at Reynolds numbers of 3200 and 21,900 (based on centerline velocity and channel half-width); statistics of the Eulerian velocity field are in good agreement with both direct numerical simulation data and experimental measurements. Single-particle Lagrangian velocity autocorrelations and particle mean-square dispersion were obtained from trajectories measured for 5000 fluid elements initially in either the viscous sublayer, buffer layer, or logarithmic region. The Lagrangian velocity autocorrelation of particles initially located in the log region decreases less rapidly than for particles initially in the buffer layer, which in turn decreases more slowly than for particles initially in the viscous sublayer. The ratio of the Lagrangian to Eulerian integral timescales were found to be proportional to the inverse of the turbulence intensity, in agreement with theoretical predictions and atmospheric measurements. Growth of particle mean-square dispersion at long diffusion times is proportional to time and in agreement with theory (with the exception of the surface-normal coordinate in which the presence of the channel wall limits dispersion). However, extremely long transport times are required to achieve the asymptotic state for the dispersion.

Key word index: Lagrangian statistics, large eddy simulation.

1. INTRODUCTION AND OBJECTIVES

One of the most basic aspects of turbulent flows is the enhanced diffusion of quantities suspended in it, e.g., heat, dye, smoke, and solid particles. Problems of turbulent diffusion span a wide range of engineering and scientific disciplines and are especially prevalent in atmospheric applications, e.g. prediction of pollutant transport. The importance of atmospheric transport is consequently reflected in an increasing research interest in transport modeling and prediction (e.g., see Mason, 1992; Sykes and Henn, 1992; Zhang and Ghoniem, 1993; Hurley and Physick, 1993; Weil, 1994). Relevant to developing accurate transport models is knowledge of the Lagrangian properties of turbulent diffusion. It is well known that turbulent diffusion is more appropriately studied within the Lagrangian frame of reference, i.e., along individual particle trajectories. Since theories of turbulent diffusion have subsequently been advanced utilizing a Lagrangian framework (Taylor, 1921; Batchelor, 1949; Corrsin, 1953, 1959), knowledge of Lagrangian statistics is central to ultimately improving prediction of turbulent transport in the atmosphere.

The principal difficulty with the Lagrangian approach to problems of turbulent diffusion is that the relevant statistical quantities are difficult to measure. Since nearly all experimental data are acquired in the fixed laboratory (Eulerian) reference frame, an important problem is then the relationship between Lagrangian statistical quantities and the more easily measured Eulerian statistics, a topic of particular interest being the relationship between Lagrangian and Eulerian timescales. Simple scaling arguments suggest that the ratio of the Lagrangian to Eulerian integral timescales, β, should be inversely proportional to the turbulence intensity i, i.e., $\beta i = \text{const.}$ (e.g., see Pasquill and Smith, 1983). Analyses lead to constants of proportionality ranging from 0.35 to 0.8 (e.g., see Saffman, 1963; Philip, 1967), while experimental evidence in the atmospheric boundary layer suggests $\beta i \approx 0.6$, though there is considerable scatter in the data. On the other hand, measurements of Lagrangian statistics in grid turbulence experiments demonstrate a Reynolds number dependence with a reduction of βi for increasing Reynolds numbers (e.g., see Sato and Yamamoto, 1987). It is not clear as to the causes of the discrepancies and detailed measurements from experiments which might shed light on these differences are not available.

Another approach for measuring Lagrangian statistics is through numerical simulation of turbulent flows. The most accurate approach is direct numerical

simulation (DNS) in which the governing equations are solved without resorting to *ad hoc* modeling at any scale. The main advantage of DNS is that it provides descriptions of turbulent flows and measurement of Lagrangian statistics is straightforward. DNS has been used by various investigators for measurement of Lagrangian statistics and the findings have for the most part corroborated those from grid turbulence experiments (e.g., see Riley and Patterson, 1974; Yeung and Pope, 1989; Squires and Eaton, 1991).

The main drawback of DNS is that it is restricted to low Reynolds numbers and therefore difficult to extrapolate to atmospheric applications. A more viable approach is large eddy simulation (LES) in which the largest, energy-containing scales of motion are computed directly while only the effects of the smallest (subgrid) scales are modeled. Since Lagrangian statistics such as the single-particle velocity autocorrelation and mean-square dispersion are strongly influenced by the large scales, LES is a viable technique for measurement of these quantities. LES was first used by Deardorff and Peskin (1970) and Peskin (1974) to obtain Lagrangian statistics in fully developed turbulent channel flow. Computer limitations constrained these studies to extremely coarse resolution of the Eulerian field (e.g., $24 \times 14 \times 20$ grid points in Deardorff and Peskin's study) as well as a relatively small ensemble of particles. LES has also been widely employed for studies of atmospheric transport, e.g., examination of particle trajectories in the atmospheric boundary layer (see Mason, 1992; Sykes and Henn, 1992). Relatively less effort has been devoted to measurement of the Lagrangian velocity autocorrelation and comparison of Lagrangian and Eulerian integral timescales.

Therefore, the specific aim of the present work is to measure Lagrangian statistical quantities, principally the single-particle velocity autocorrelation and mean-square dispersion, in a well-defined turbulent shear flow: fully developed turbulent channel flow. Turbulent flow in a channel bounded by smooth parallel walls is a highly idealized approximation to the atmospheric boundary layer. However, the turbulent channel flow considered in this work does possess some similarities to the atmospheric boundary layer (e.g., to the constant-stress surface layer). Thus, it should then be possible to generalize the findings reported in this work to atmospheric flows.

The approach adopted in the present study is large eddy simulation of the incompressible Navier–Stokes equations. Important in this regard is a subgrid-scale (SGS) model in the LES calculations which can account for changes in resolution as the Reynolds number is varied. Therefore, in this work the dynamic eddy viscosity model is used to parametrize SGS stresses (Germano *et al.*, 1991). Use of the dynamic model is particularly well suited for this work since the eddy viscosity is calculated during the course of the computation. Thus, the model can respond to changes in the spectral content of the turbulence as the Reynolds number is changed without *ad hoc* tuning. Turbulent channel flow is statistically stationary with a single inhomogeneous direction normal to the channel walls and, therefore, Lagrangian statistical quantities are a function of time separation as well as the initial location of particles relative to the surface. In this work Lagrangian statistics were obtained for particles with initial locations in three regions of the channel: the viscous sublayer, buffer layer, and logarithmic region. Contained in Section 2 is a description of the simulation technique together with properties of the Eulerian velocity fields. Lagrangian statistics obtained from the simulations may be found in Section 3 and a summary of the work is provided in Section 4.

2. SIMULATION OVERVIEW

2.1. *LES of turbulent channel flow*

The filtered Navier–Stokes equations governing fully developed turbulent channel flow driven by a uniform streamwise pressure gradient are

$$\frac{\partial \bar{u}_i}{\partial x_i} = 0, \tag{1}$$

$$\frac{\partial \bar{u}_i}{\partial t} + \frac{\partial}{\partial x_j}(\bar{u}_i \bar{u}_j) = -\frac{\partial \bar{p}}{\partial x_i} + \frac{1}{Re_\tau}\frac{\partial^2 \bar{u}_i}{\partial x_j \partial x_j} - \frac{\partial \tau_{ij}}{\partial x_j} + \delta_{i1}, \tag{2}$$

where u_i is the fluid velocity, p is the pressure, δ_{ij} is the Kronecker delta, and $i = 1, 2, 3$ refers to the x (streamwise), z (surface-normal) and y (spanwise) directions, respectively (the usual summation notation applies and an overbar denotes application of the filtering operation). The governing equations (1) and (2) have been made dimensionless using the channel half-width δ and friction velocity u_τ. The Reynolds number in equation (2) is then $Re_\tau = u_\tau \delta / \nu$, where ν is the kinematic viscosity. For fully developed channel flow periodic boundary conditions for the dependent variables are applied in the streamwise and spanwise directions whereas the no-slip condition is applied on the channel walls.

The effect of the small scales on the energy-containing eddies in equation (2) is represented by the SGS stress, $\tau_{ij} = \overline{u_i u_j} - \bar{u}_i \bar{u}_j$, which requires a model and in this work τ_{ij} is parametrized using an eddy viscosity hypothesis

$$\tau_{ij} - \tfrac{1}{3}\delta_{ij}\tau_{kk} = -2\nu_T \bar{S}_{ij}, \tag{3}$$

where the eddy viscosity is $\nu_T = C\bar{\Delta}^2|\bar{S}|$, the resolved-scale strain rate tensor is defined as $\bar{S}_{ij} = 0.5(\partial \bar{u}_i/\partial x_j + \partial \bar{u}_j/\partial x_i)$, and $|\bar{S}| = \sqrt{2\bar{S}_{ij}\bar{S}_{ij}}$ is the

magnitude of $\bar{S}_{ij}$. The filter width is defined as $\bar{\Delta}(z) = (\bar{\Delta}_1\bar{\Delta}_2(z)\bar{\Delta}_3)^{1/3}$, where $\bar{\Delta}_1$, $\bar{\Delta}_2$, and $\bar{\Delta}_3$ are the grid spacing in the x, z, and y directions, respectively. The model coefficient C requires specification in order to close the system (1) and (2). In this work the model coefficient is determined dynamically from the resolved sales following the procedure outlined by Germano *et al.* (1991) and is calculated using the least-squares approach of Lilly (1992). The governing equations (1) and (2) were solved numerically using the fractional step method on a staggered gird (e.g., see Kim and Moin, 1985; Wu *et al.*, 1995).

Calculations of channel flows were performed at two Reynolds numbers for which DNS results and experimental measurements of the Eulerian velocity field are available. The calculations will be referred to in this work as the "low Reynolds number simulation" at $Re_\tau = 180$ and "high Reynolds number simulation" at $Re_\tau = 1000$, corresponding to the Reynolds number, Re_c, based on channel centerline velocity of 3200 and 21,900, respectively. For both the low and high Reynolds number simulations the Navier–Stokes equations were resolved using $64 \times 65 \times 64$ grid points (65 points in the surface-normal direction). The channel domain for the low Reynolds number calculations was $4\pi\delta \times 2\delta \times 4\pi\delta/3$ and $5\pi\delta/2 \times 2\delta \times \pi\delta/2$ for the high Reynolds number flow. Previous computations of turbulent channel flow have shown these domain sizes are sufficient to ensure that the solution is not adversely affected by periodic boundary conditions (Piomelli, 1993). The grid spacing in wall coordinates in the x and y directions was $\Delta x^+ = 35$ and $\Delta y^+ = 12$ for the low Reynolds number case and $\Delta x^+ = 123$ and $\Delta y^+ = 25$ for the high Reynolds number simulations. Note that non-dimensionalization in terms of the friction velocity u_τ and viscosity ν are denoted with a $+$ superscript, e.g., $x^+ = xu_\tau/\nu$. A stretched grid was used in the surface-normal direction and for both Reynolds numbers the first grid point was at $z^+ < 1$. After a statistically stationary condition was obtained, statistical quantities were sampled for $3\delta/u_\tau$ and $8\delta/u_\tau$ for the low and high Reynolds number simulations, respectively.

Shown in Fig. 1 is the mean velocity profile in both channel and wall coordinates for the low and high Reynolds number calculations. Figure 1a demonstrates good agreement between the mean velocity profile obtained in the low Reynolds number simulations with the DNS results of Kim *et al.* (1987). Figure 1b shows the existence of a logarithmic layer for both simulations; good agreement between the LES predictions at $Re_\tau = 180$ and the DNS data are again evident. Comparison of the LES results for the high Reynolds number simulation demonstrate reasonable agreement with the boundary layer measurements of Balint *et al.* (1991) at a comparable Reynolds number ($Re_\delta = 23{,}000$ based on freestream velocity and boundary layer thickness in the experiment).

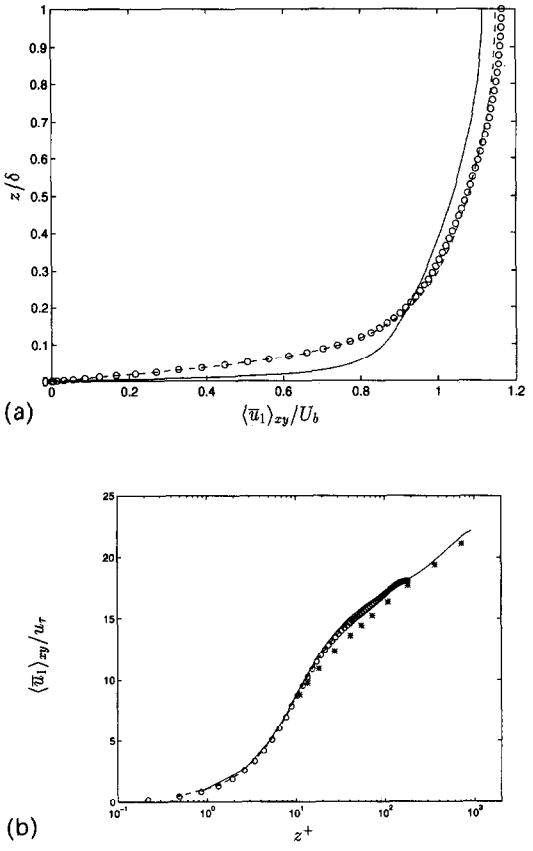

Fig. 1. Mean velocity profile in (a) global coordinates and (b) wall coordinates. Mean profile in (a) has been normalized by the bulk velocity $U_b = 0.5\int_{-1}^{1}\langle\bar{u}_1\rangle_{xy}\,dz$. LES: (- - - -) $R_\tau = 180$; (———) $R_\tau = 1000$; (o) Kim *et al.* (1987); (*) Balint *et al.* (1991).

Turbulence intensities from the low and high Reynolds number simulations are shown in Fig. 2. Good agreement between the LES predictions and DNS results for the low Reynolds number simulations may be observed in Fig. 2a. Shown in Fig. 2b is a comparison of the turbulence intensities from the high Reynolds number calculations to the experimental measurements of Wei and Willmarth (1989). The experimental data were obtained at a channel flow Reynolds number $Re_c = 23{,}000$; Figure 2b shows that the present LES calculations agree reasonably well with the experimental measurements.

2.2 *Calculation of particle trajectories*

Given an Eulerian velocity field calculated as described in Section 2.1, the trajectories of a number of tagged particles are followed as the flow evolves. Let $X_\alpha(x_\alpha^0, t)$ denote the position of the fluid particle which is located at x_α^0 at the initial time t_0, i.e.,

$$X_\alpha(x_\alpha^0, t_0) = x_\alpha^0, \tag{4}$$

(no summation is applied for repeated Greek indices). The Lagrangian velocity of a fluid particle $V_\alpha(x_\alpha^0, t)$ is

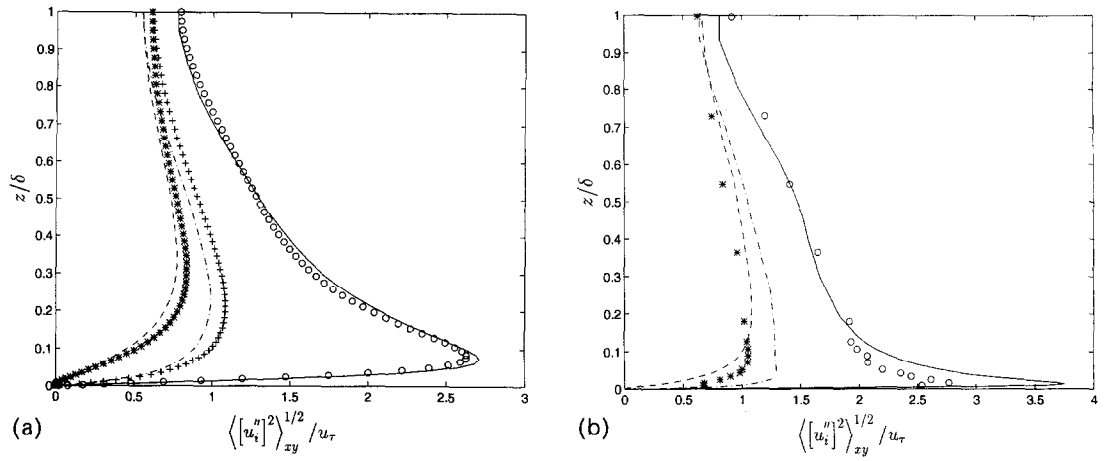

Fig. 2. Root-mean square fluctuating velocity $\langle [u''_i]^2 \rangle_{xy}^{1/2}$, where $u''_i(t, x, z, y) = \tilde{u}_i(t, x, z, y) - \langle \bar{u}_i(t, x, z, y) \rangle_{xy}$. (a) LES ($R_\tau = 180$): (———) streamwise; (- - - -) surface normal; (– · –) spanwise; Kim *et al.* (1987); (o) streamwise; (*) surface-normal; (+) spanwise. (b) LES ($R_\tau = 1000$): (———) streamwise; (- - - -) surface-normal; (– · –) spanwise; Wei and Willmarth (1989): (o) streamwise; (*) surface-normal.

then the Eulerian velocity at the particle position

$$V_\alpha(x_\alpha^0, t) = \tilde{u}_\alpha[X_\alpha(x_\alpha^0, t), t]. \tag{5}$$

Particle displacement is obtained using

$$\frac{\partial X_\alpha(x_\alpha^0, t)}{\partial t} = V_\alpha(x_\alpha^0, t). \tag{6}$$

To simplify notation, dependence on the initial particle position x_α^0 is implied but will be subsequently omitted from the expressions for the position and velocity, i.e., $X_\alpha(x_\alpha^0, t)$ and $V_\alpha(x_\alpha^0, t)$ shall be expressed as $X_\alpha(t)$ and $V_\alpha(t)$, respectively. Particle positions were advanced using second-order Adams–Bashforth and the velocity at the particle position was obtained using fourth-order Lagrange polynomial interpolation [see Wang *et al.* (1994) for further discussion].

Note that if a particle moves out of the computational domain in the streamwise or spanwise directions, periodic boundary conditions are used to obtain the velocity of the particle whereas the actual dispacement is used for calculating particle dispersion.

After obtaining a statistically stationary Eulerian velocity field, the initial streamwise and spanwise locations of the particles were assigned randomly in planes parallel to the wall in the viscous sublayer, buffer layer, and log region. The velocity and displacement of the particles were used to compute the quantities of primary interest in this study: the single-particle Lagrangian velocity autocorrelation and particle mean-square dispersion. For flows in which the inhomogeneous direction is the surface-normal coordinate z, the Lagrangian velocity correlation coefficient is defined as

$$R_{ij}^{\mathrm{L}}(\tau, z_0) = \frac{\langle [V_i(t_0) - \tilde{u}_i(t_0, z_0)][V_j(t_0 + \tau) - \tilde{u}_j(t_0 + \tau, X_2(t_0 + \tau))] \rangle}{\langle [V_i(t_0) - \tilde{u}_i(t_0, z_0)]^2 \rangle^{1/2} \langle [V_j(t_0 + \tau) - \tilde{u}_j(t_0 + \tau, X_2(t_0 + \tau))]^2 \rangle^{1/2}}, \tag{7}$$

where $\tilde{u}_i(t, z) = \langle \bar{u}_i(t, x, z, y) \rangle_{xy}$ is the plane-averaged velocity and the angle brackets $\langle\ \rangle$ denote averaging over all particles initially located in the same x–y plane. Note that since the particles were tracked only after the flow has become statistically stationary the correlations are independent of the initial time t_0. Since a question of fundamental interest is the relationship between Lagrangian and Eulerian statistics, the Eulerian temporal correlation was also calculated

$$R_{ij}^{\mathrm{E}}(\tau, z_0) = \frac{\langle [\bar{u}_i(t_0, z_0) - \tilde{u}_i(t_0, z_0)][\bar{u}_j(t_0 + \tau, z_0) - \tilde{u}_j(t_0 + \tau, z_0)] \rangle_{xy}}{\langle [\bar{u}_i(t_0, z_0) - \tilde{u}_i(t_0, z_0)]^2 \rangle_{xy}^{1/2} \langle [\bar{u}_j(t_0 + \tau, z_0) - \tilde{u}_j(t_0 + \tau, z_0)]^2 \rangle_{xy}^{1/2}}. \tag{8}$$

Particle dispersion was calculated from

$$\langle Z_\alpha Z_\alpha \rangle(\tau, z_0) = \langle [X_\alpha(t_0 + \tau) - X_\alpha(t_0) - \langle X_\alpha(t_0 + \tau) - X_\alpha(t_0) \rangle]^2 \rangle. \tag{9}$$

Defining the dispersion as in (9) should lead to asymptotic growth in $\langle Z_\alpha Z_\alpha \rangle$ which is directly proportional to time (e.g., see Monin and Yaglom, 1971).

3. LAGRANGIAN STATISTICS

3.1. *Velocity autocorrelations*

For the low Reynolds number simulation fluid particles were initially assigned random streamwise and spanwise coordinates in x–y planes at $z^+ = 2.4$ (viscous sublayer), $z^+ = 18$ (buffer layer), and $z^+ = 93$ (log region) while for the high Reynolds number calculation particles were initially located in x–y planes at $z^+ = 2.7$ (viscous sublayer), $z^+ = 32$ (buffer layer), and $z^+ = 298$ (log region). For each plane in which particles were initially located, statistics were obtained by ensemble averaging over 5000 trajectories. Numerical experiments demonstrated adequate statistical convergence was obtained using this sample size [see Wang *et al.* (1994) for further discussion].

3.1.1. *Low Reynolds number simulation.* The velocity autocorrelation coefficients for particles initially located in the viscous sublayer, buffer layer, and log region are presented in Fig. 3. Note that the cross-correlation coefficients R^L_{12} have been normalized by the value at $t = 0$. It is clear from Fig. 3 that the autocorrelations in the streamwise direction decreases less rapidly than those in either the spanwise or surface-normal directions for all initial particle locations. Similar behavior in the correlation coefficients was first observed by Deardorff and Peskin (1970) in the outer region of turbulent channel flow as well as in later simulations of homogeneous turbulent shear flow by Squires and Eaton (1991). The present study demonstrates this effect is apparent throughout the channel. It is also evident that the correlations of particles initially located in the log region decrease more slowly than those in the buffer layer, which in turn decrease less rapidly than those in the viscous sublayer. The increase in the correlation coefficient with increasing distance from the wall is presumably linked to the increase in scale of eddies at larger distances from the wall.

From the autocorrelation coefficients shown in Fig. 3 it is possible to calculate the Lagrangian integral timescale,

$$T^L_{ij} = \int_0^{t_f} R^L_{ij}(\tau)\,\mathrm{d}\tau, \tag{10}$$

where $t_f \gg T^L_{ij}(t_f = 3\delta/u_\tau$ in the present study). Extraction of T^L_{ij} from simulation data or experimental measurements can be somewhat ambiguous since calculation of the integral scale may exhibit a dependence of t_f (e.g., through extended oscillations about zero). A slightly less ambiguous measure is the time T^{Le}_{ij} required for the velocity correlation coefficient to decrease to $1/e$, i.e., $R^L_{ij}(T^{Le}_{ij}) = 1/e$. One of the principal uses of the timescales (10) and T^{Le}_{ij} for studies of turbulent diffusion is that the Lagrangian autocorrelation is often approximated as a decaying exponential, i.e, $\exp(-t/T^L_{ij})$ and $\exp(-t/T^{Le}_{ij})$ (e.g., see Sawford 1982, 1984). Shown in Fig. 4 is a comparison of the Lagrangian velocity autocorrelations, the exponential curves $\exp(-t/T^L_{ij})$ and $\exp(-t/T^{Le}_{ij})$, and the Eulerian temporal correlations measured at fixed spatial locations. Several interesting observations can be made from the figure. First, while both the exponential curve $\exp(-t/T^L_{ij})$ and $\exp(-t/T^{Le}_{ij})$ are

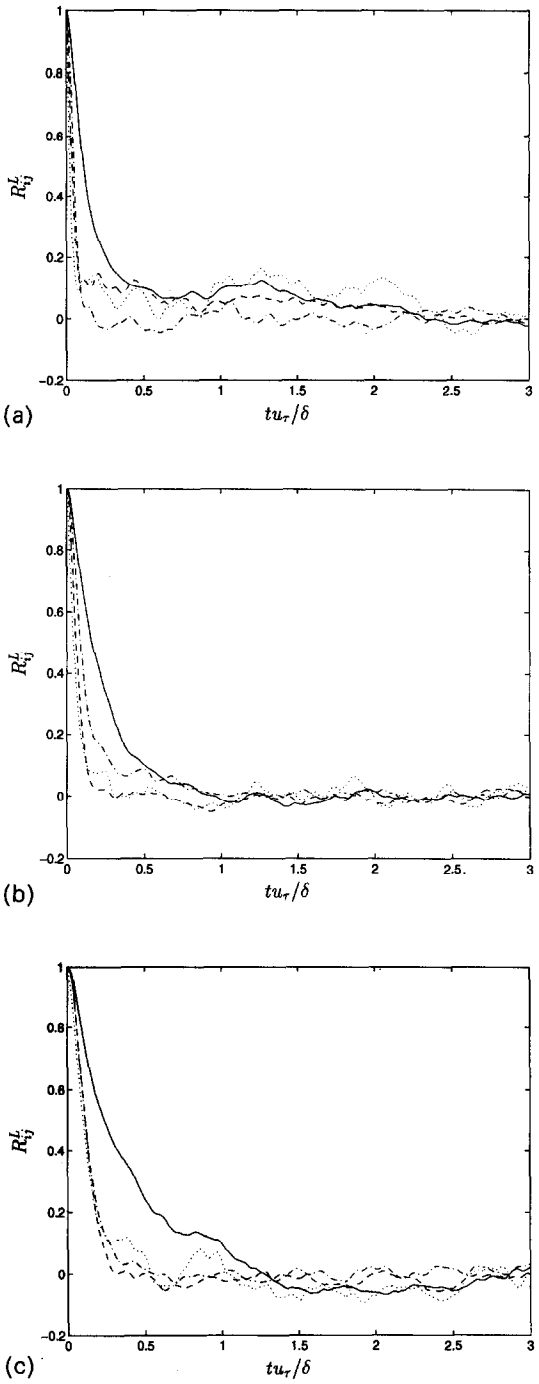

Fig. 3. Lagrangian velocity autocorrelation coefficients in turbulent channel flow, $R_\tau = 180$. Initial particle locations: (a) viscous sublayer, (b) buffer layer, (c) log region. (——) R^L_{11}; (- - -) R^L_{22}; (–·–) R^L_{33}; (·····) R^L_{12} (cross-correlation has been normalized by its value at $t = 0$).

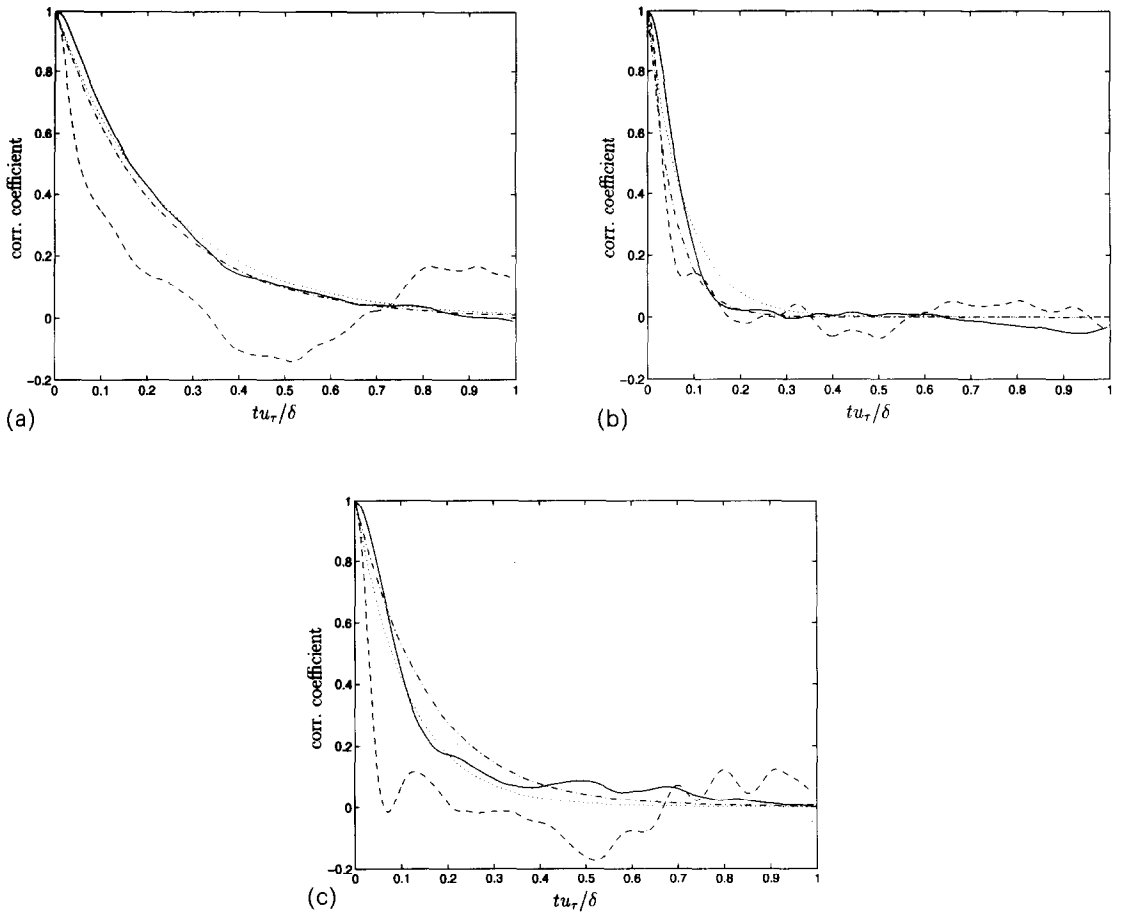

Fig. 4. Velocity autocorrelations in turbulent channel flow, particles initially located in buffer layer, $R_\tau = 180$. (a) streamwise; (b) surface-normal; (c) spanwise. (- - - -) Eulerian; (———) Lagrangian; (– · –) exp $(-t/T_{ij}^{\mathrm{L}})$; (·····) exp $(-t/T_{ij}^{\mathrm{Le}})$.

reasonable approximations of the Lagrangian velocity autocorrelations, the curve $\exp(-t/T_{ij}^{\mathrm{Le}})$ appears to better represent R_{ij}^{L} for the majority of the measurements. Second, the Eulerian velocity correlations are always smaller than the Lagrangian velocity correlations for small time separations. As shown in Table 1 the ratio of the Lagrangian integral timescale to the Eulerian integral scale varies from 1.3 to over 10 (with the exception of the integral scales obtained from the cross-correlations).

Table 1. Ratio of the Lagrangian integral timescale to Eulerian timescale for the low Reynolds number simulation, $R_\tau = 180$. Average value of the ratio for the diagonal components is 3.41

	$y^+ = 2.4$	$y^+ = 18$	$y^+ = 93$
$T_{11}^{\mathrm{Le}}/T_{11}^{\mathrm{Ee}}$	1.43	2.52	10.25
$T_{12}^{\mathrm{Le}}/T_{12}^{\mathrm{Ee}}$	0.33	0.56	2.00
$T_{22}^{\mathrm{Le}}/T_{22}^{\mathrm{Ee}}$	1.33	1.86	5.33
$T_{33}^{\mathrm{Le}}/T_{33}^{\mathrm{Ee}}$	1.33	3.17	5.33

For a statistically stationary flow with a single direction of inhomogeneity it is also convenient to define the Lagrangian mean and fluctuating velocity by ensemble averaging over the particles (e.g., see Hinze, 1975). In this case the Lagrangian velocity autocorrelation is defined as

$$R_{ij}^{\mathrm{L}}(\tau, z_0) = \frac{\langle [V_i(t_0) - \langle V_i(t_0)\rangle][V_j(t_0+\tau) - \langle V_j(t_0+\tau)\rangle]\rangle}{\langle [V_i(t_0) - \langle V_i(t_0)\rangle]^2\rangle^{1/2}\langle [V_j(t_0+\tau) - \langle V_j(t_0+\tau)\rangle]^2\rangle^{1/2}}, \qquad (11)$$

where the principal difference between equations (11) and (7) is that the Lagrangian fluctuating velocity has been obtained by subtracting the mean value obtained via an ensemble average. Note that this will affect only the computation of the streamwise correlations. Comparison of the streamwise components of the velocity autocorrelation from equations (11) and (7) is shown in Fig. 5. Use of ensemble averages over the particles to define the Lagrangian mean velocity

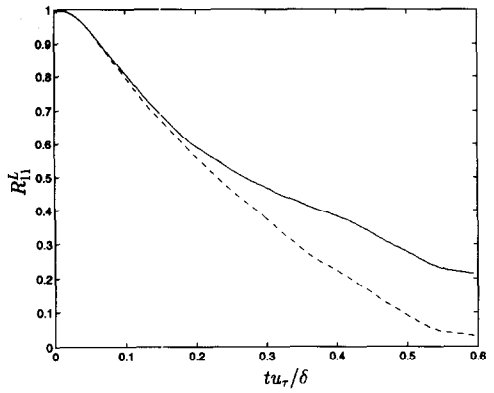

Fig. 5. Streamwise component of Lagrangian velocity autocorrelation, $R_\tau = 180$. Particles initially located in the buffer layer. (———) equation (7); (- - - -) equation (11).

effectively reduces the correlation as may be observed in Fig. 5. It was found that the resultant decrease in the integral timescale is approximately 20–25%.

3.1.2. *High Reynolds number simulation.* Shown in Fig. 6 are the Lagrangian velocity autocorrelations R_{ij}^L from the high Reynolds number simulations. Similar to the low Reynolds number case, the correlation coefficient decreases more rapidly for particles initially located in the viscous sublayer than in the buffer layer and log region. Furthermore, as also observed in Fig. 3, there is a greater persistence in the correlation of streamwise particle velocities than in either the spanwise or surface-normal directions.

Lagrangian and Eulerian autocorrelations from the high Reynolds number simulation are shown in Fig. 7. Similar to the low Reynolds number case, $\exp(-t/T_{ij}^{Le})$ is a more accurate approximation of the Lagrangian velocity autocorrelation R_{ij}^L than $\exp(-t/T_{ij}^L)$ for most of the components. As also observed at the lower Reynolds number, the Eulerian velocity correlations decrease more rapidly than the Lagrangian correlations for small time separations. Shown in Table 2 is the ratio of the Lagrangian integral timescale to the corresponding Eulerian integral scales. The values shown in Table 2 are in qualitative agreement with those obtained from the low Reynolds number calculations, e.g., the ratios vary over nearly the same range, 1.3–8.9, at the higher Reynolds number. The average value of the ratios for the diagonal components is 3.6, nearly the same as that obtained at the lower Reynolds number.

The results in Tables 1 and 2 demonstrate that for both Reynolds numbers considered in this work there is a greater persistence of the correlation measured along particle trajectories relative to those obtained in the fixed Eulerian reference frame. Similar behavior has been observed in other studies of turbulent diffusion (e.g., see Hay and Pasquill, 1959; Deardorff and Peskin, 1970; Sato and Yamamoto, 1987). Advection by the mean flow has a direct effect on the timescales and as shown, for example, in Pasquill and Smith

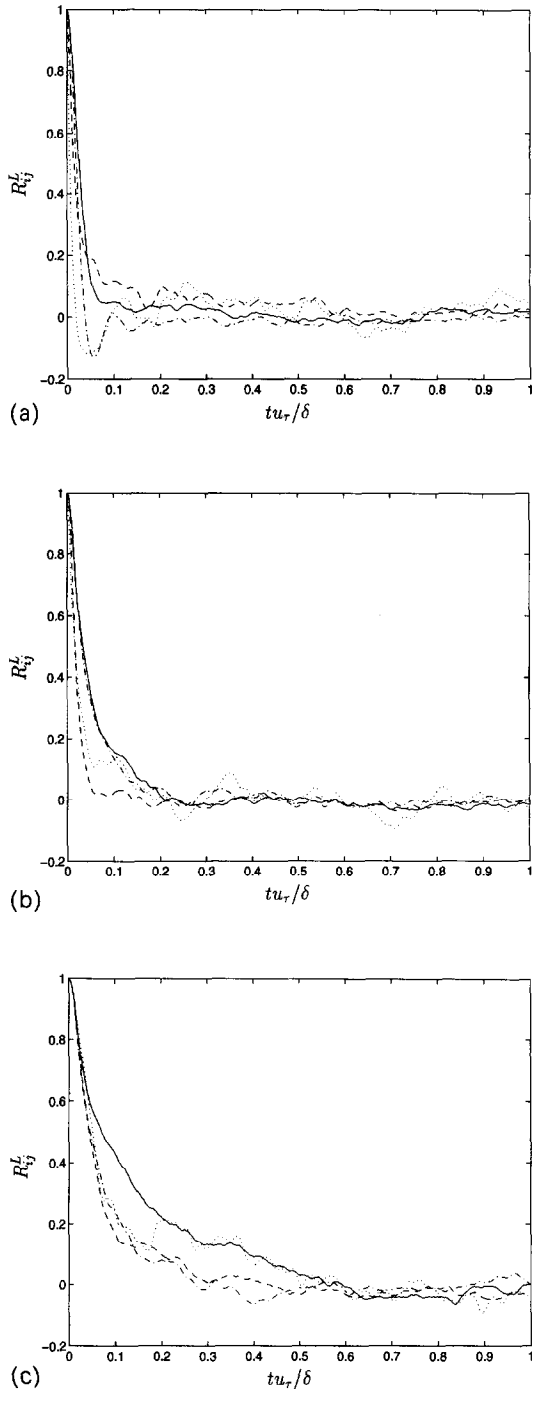

Fig. 6. Lagrangian velocity autocorrelation coefficients in turbulent channel flow, $R_\tau = 1000$. Initial particle locations: (a) viscous sublayer, (b) buffer layer (c) log region. (———) R_{11}^L; (- - - -) R_{22}^L; (— · —) R_{33}^L; (·····) R_{12}^L (cross-correlation has been normalized by its value at $t = 0$).

(1983), the ratio of the Lagrangian to Eulerian integral timescales, β, is dependent on the turbulence intensity i,

$$i = \frac{\langle [\bar{u}_i(t, x, z, y) - \langle \bar{u}_i(t, x, z, y)\rangle_{xy}]^2\rangle_{xy}^{1/2}}{\langle \bar{u}_i(t, x, z, y)\rangle_{xy}}. \quad (12)$$

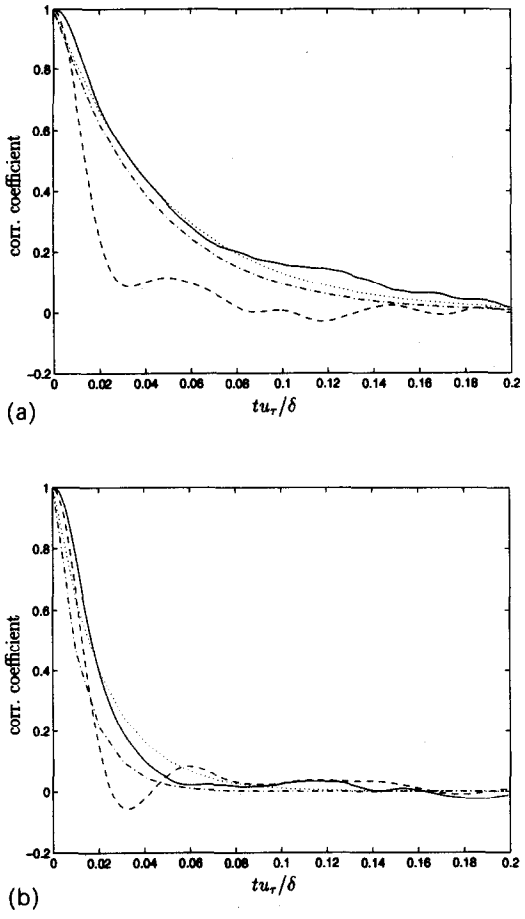

Fig. 7. Velocity autocorrelations in turbulent channel flow, particles initially located in buffer layer, $R_\tau = 1000$. (a) streamwise; (b) surface-normal; (c) spanwise. (- - - -) Eulerian; (———) Lagrangian; (– · · –) $\exp(-t/T^{L}_{ij})$; (·····) $\exp(-t/T^{Le}_{ij})$.

Atmospheric measurements have shown an approximate linear increase in β with increases in $1/i$ (e.g., see Angell, 1964; Hanna, 1981). Theoretical estimates yield $\beta i \approx$ const. with constants ranging from 0.35 to 0.8 (e.g., see Philip, 1967; Saffman, 1963; Pasquill and Smith, 1983). Experimental measurements in grid turbulence also show that β increases with $1/i$, though the βi decreases with increases in the Reynolds number. Sato and Yamamoto (1987) found that βi decreased from 0.6 to 0.3 for increasing Reynolds number. The ratio of the Lagrangian to Eulerian integral timescales as a function of $1/i$ is shown in Fig. 8 (the timescales shown in the figure have been averaged over the three coordinate directions). The present results appear to support $\beta i \approx 0.6$, in agreement with atmospheric data and analyses.

Table 2. Ratio of the Lagrangian integral timescale to Eulerian timescale for the high Reynolds number simulation, $Re_\tau = 1000$. Average value of the ratio for diagonal components is 3.62

	$y^+ = 2.7$	$y^+ = 32$	$y^+ = 298$
T^{Le}_{11}/T^{Ee}_{11}	1.57	2.88	8.93
T^{Le}_{12}/T^{Ee}_{12}	0.22	0.36	2.10
T^{Le}_{22}/T^{Ee}_{22}	1.31	1.38	5.00
T^{Le}_{33}/T^{Ee}_{33}	1.26	2.81	5.58

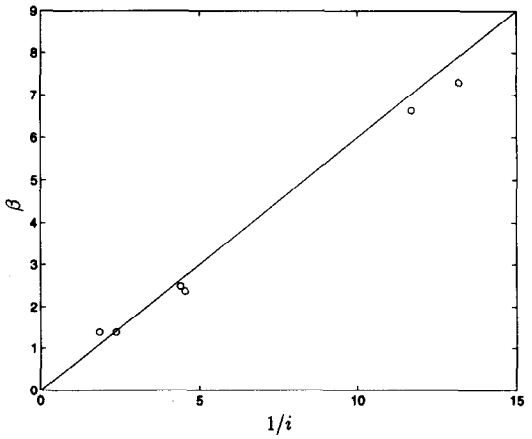

Fig. 8. Ratio of Lagrangian to Eulerian integral timescale. (o) LES; (———) $\beta i = 0.6$.

3.2. *Particle dispersion*

Mean-square dispersion $\langle Z_\alpha Z_\alpha \rangle$ for particles from the high Reynolds number simulation are shown in Fig. 9 (for brevity, only the results from the high Reynolds number calculation are shown in this section). Consistent with the ratios of component energies in wall-bounded flows, Fig. 9 shows that the streamwise dispersion is larger than the spanwise component which is in turn larger than the dispersion in the surface-normal direction. It is also evident that for short diffusion times mean-square dispersion $\langle Z_\alpha Z_\alpha \rangle$ is proportional to t^2, consistent with the predictions of Taylor (1921) and results obtained in homogeneous turbulence (e.g., see Riley and Patterson, 1974; Yeung and Pope, 1989; Squires and Eaton,

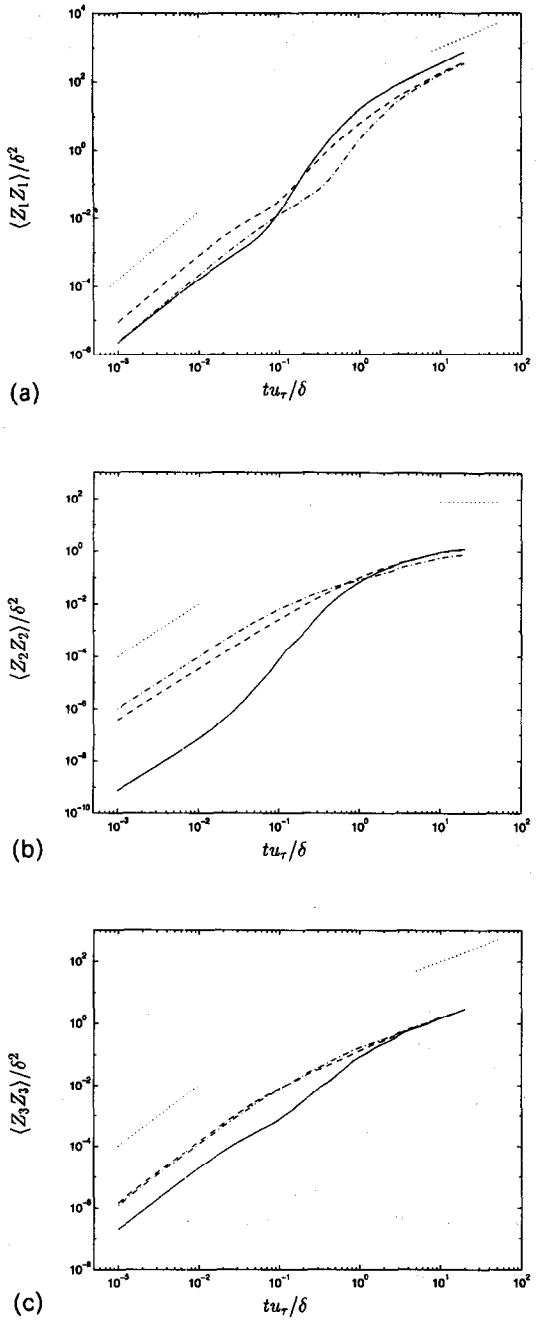

Fig. 9. Particle mean-square dispersion $\langle Z_\alpha Z_\alpha\rangle$ in turbulent channel flow, $R_\tau = 1000$. Particles initially located in viscous sublayer (———), buffer layer (- - -), and log region (– · –); (·····) t^2 (small time separations); (a) $\langle Z_1Z_1\rangle$; (·····) t^1; (b) $\langle Z_2Z_2\rangle$; (·····) t^0; (c) $\langle Z_3Z_3\rangle$; (·····) t^1.

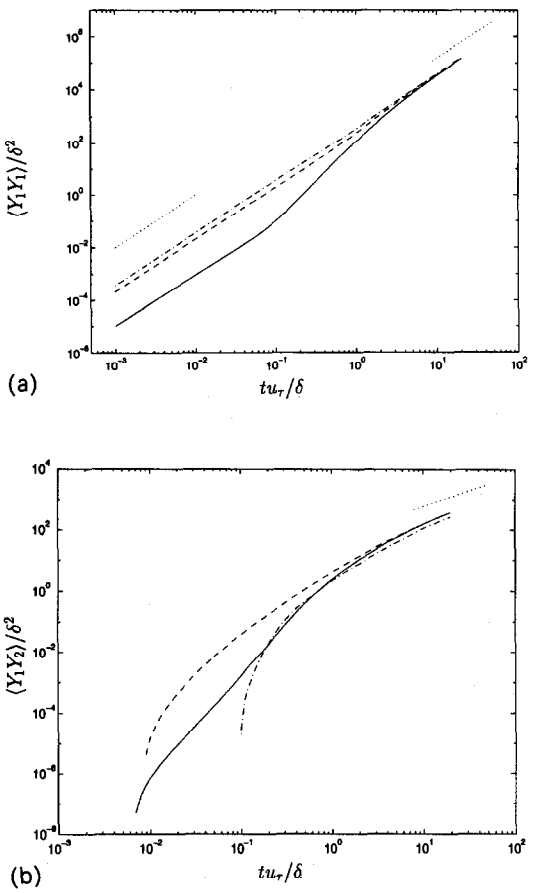

Fig. 10. Particle mean-square dispersion in turbulent channel flow, $R_\tau = 1000$. Particles initially located in the viscous sublayer (———), buffer layer (- - -), and log region (– · –). (a) $\langle Y_1Y_1\rangle$, (·····) t^2; (b) $\langle Y_1Y_2\rangle$, (·····) t^1;

1991). At short diffusion times the mean-square dispersion is proportional to the velocity variance and the relative levels of the dispersion in Fig. 9 are consistent with the magnitude of the component velocity fluctuations. At long travel times particle transport is limited by the presence of the channel walls and fluid elements eventually become uniformly distributed throughout the channel. Thus, asymptotic dispersion should become independent of the initial particle location (with the exception of the inhomogeneous surface-normal direction). The results in Fig. 9 shows that the spanwise component $\langle Z_3Z_3\rangle$ appears to reach the asymptotic condition after approximately $10\delta/u_\tau$, corresponding to over 100 integral timescales. It is also clear from Fig. 9 that at long travel times $\langle Z_3Z_3\rangle$ is directly proportional to time. However, the streamwise component of dispersion does not demonstrate a similar independence of initial location, though the asymptotic growth does appear to be $\langle Z_1Z_1\rangle \propto t$. It may also be observed from Fig. 9 that dispersion of particles initially located in the viscous sublayer increases at a substantially faster rate than for particles in either the buffer or log layers. Particles can be moved relatively far from the sublayer which in turn results in substantially rapid increases in dispersion.

The effect of the mean-flow on dispersion, not included in the results shown in Fig. 9, was examined through calculation of

$$\langle Y_iY_j\rangle(\tau, z_0) = \langle [X_i(t_0+\tau) - X_i(t_0)][X_j(t_0+\tau) - X_j(t_0)]\rangle. \quad (13)$$

In stationary homogeneous shear flow Corrsin (1953, 1959) showed that $\langle Y_1 Y_1 \rangle$ should grow proportional to t^3 at long diffusion times. Squires and Eaton (1991) found that in non-stationary homogeneous shear flow that the time-dependence of $\langle Y_1 Y_1 \rangle$ was closer to $t^{3.3-3.6}$. Particle mean-square dispersion $\langle Y_1 Y_1 \rangle$ from the channel flow simulations is shown in Fig. 10a (note that $\langle Y_2 Y_2 \rangle = \langle Z_2 Z_2 \rangle$ and $\langle Y_3 Y_3 \rangle = \langle Z_3 Z_3 \rangle$). As expected, for short diffusion times $\langle Y_1 Y_1 \rangle$ increases according to t^2. At long travel times particle motion becomes independent of the initial location and particle dispersion $\langle Y_1 Y_1 \rangle$ becomes independent of the initial positions at $t \approx 10\delta/u_\tau$. Unlike dispersion in homogeneous flows, however, the asymptotic growth of particle dispersion in the channel is less than in homogeneous turbulence. Because the velocity is bounded the long-time growth of $\langle Y_1 Y_1 \rangle$ varies as t^2 in the channel (for $t > 10\delta/u_\tau$). The cross-component of dispersion $\langle Y_1 Y_2 \rangle$ for particles initially located in different x–y planes is shown in Fig. 10b. At long diffusion times $\langle Y_1 Y_2 \rangle \propto t^2$ in stationary homogeneous shear flow. However, similar to the streamwise component, the bounded nature of the velocity field imposed by the channel walls effectively reduces the asymptotic behavior of $\langle Y_1 Y_2 \rangle$. The results in Fig. 10a show that $\langle Y_1 Y_2 \rangle \propto t^1$.

4. SUMMARY

Large eddy simulations were carried out and single-particle Lagrangian statistics obtained for turbulent channel flows at Reynolds numbers $Re_\tau = u_\tau \delta/\nu = 180$ and $Re_\tau = 1000$, corresponding to $Re_c = U_c \delta/\nu = 3200$ and $Re_c = 21{,}900$, respectively. Particles were initially distributed in x–y planes at three surface-normal locations. Similar to homogeneous shear flow, Lagrangian velocity autocorrelations in the streamwise direction decrease less rapidly than either the spanwise or surface-normal components; the present study indicates this behavior is inherent to turbulent shear flows. Lagrangian integral timescales increase with increasing distance from the wall and are, on average, 3–4 times larger than the corresponding integral timescales obtained from fixed-point Eulerian correlations. Further, the product of the timescale ratio and turbulence intensity is approximately 0.6 at both Reynolds numbers and in reasonable agreement with analyses and atmospheric measurements. The fact that the timescale ratios from the present simulations at moderate Reynolds numbers are in reasonable agreement with results previously obtained from atmospheric studies would seem to demonstrate some universality in this finding. Further, the work reported here should also enhance stochastic models of turbulent diffusion. This study shows that the Lagrangian velocity autocorrelation may be represented with using a decaying exponential and the integral timescale in turbulent shear flows can be reasonably approximated from $\beta i \approx 0.6$.

Finally, it should be remarked that in the present study Lagrangian statistics were obtained from the resolved velocity field, effects of subgrid-scale velocities on statistical quantities were not considered. While neglect of subgrid-scale velocities on two-particle statistics would introduce large errors, especially at short diffusion times, single-particle quantities such as the velocity autocorrelation are significantly less sensitive to the subgrid scale velocity field. Furthermore, accurate modeling of the subgrid-scale stress in large eddy simulation requires that there be adequate separation between the large scales corresponding to the peak of the spectrum, and the smallest resolved scales defined by the cut-off wave number of the computation. Quantities such as the integral scales are much more dependent on the peak of the spectrum relative to the contribution of the subgrid-scale field and therefore it is not expected that quantities such as the integral timescales will be significantly altered by their inclusion. Preliminary calculations not reported here indicate that modeling the effect of subgrid-scale velocities on the Lagrangian statistics presented in this paper yields changes in integral quantities of only a few percent.

Acknowledgement—This work is supported by the National Institute Occupational Safety and Health (Grant Number OH03052-02) and the Office of Naval Research (Grant Number N00014-94-1-0047). Computer time for the simulations was supplied by the Cornell Theory Center.

REFERENCES

Angell J. K. (1964) Measurements of Lagrangian and Eulerian properties of turbulence at a height of 2300 ft. *Q. J. R. Met. Soc.* **90**, 57.

Balint J.-L., Wallace J. M. and Vukoslavcevic P. (1991) The velocity and vorticity vector fields of a turbulent boundary layer. Part 2. Statistical properties. *J. Fluid Mech.* **228**, 53–86.

Batchelor G. K. (1949) Diffusion in a field of homogeneous turbulence. *Aus. J. Sci. Res.* **2**, 437–450.

Corrsin S. (1953) Remarks on turbulent heat transfer. *Proc. Iowa Thermodynamics Symp.* University of Iowa, Iowa City, Iowa, pp. 5–30.

Corrsin S. (1959) Progress report on some turbulent diffusion research. *Adv. Geophys.* **6** (Atmospheric diffusion and air pollution), 161–164.

Deardorff J. W. and Peskin R. L. (1970) Lagrangian statistics from numerically integrated turbulent shear flow. *Phys. Fluids* **13**, 584–595.

Germano M., Piomelli U., Moin P. and Cabot W. H. (1991) A dynamic subgrid scale eddy viscosity model. *Phys. Fluid* **A3**, 1760–1765.

Hanna R. S. (1981) Lagrangian and Eulerian time-scale relations in the daytime boundary layer. *J. Appl. Met.* **20**, 242–249.

Hay J. S. and Pasquill F. (1959) Diffusion from a continuous source in relation to the spectrum and scale of turbulence. *Adv. Geophys.* **6** (Atmospheric diffusion and air pollution), 345–365.

Hinze J. O. (1975) *Turbulence.* McGraw-Hill, New York.

Hurley P. and Physick W. (1993) Lagrangian particle modelling of buoyant point sources: plume rise and entrapment

under convective conditions. *Atmospheric Environment* **27**, 1579.

Kim J. and Moin P. (1985) Application of a fractional-step method to incompressible Navier–Stokes equations. *J. Comput. Phys.* **59**, 308–323.

Kim J., Moin P. and Moser R. (1987) Turbulence statistics in fully developed channel flow at low Reynolds number. *J. Fluid Mech.* **177**, 133–166.

Lilly D. K. (1992) A proposed modification of the Germano subgrid-scale closure method. *Phys. Fluid* **A4**, 633–635.

Mason P. J. (1992) Large-eddy simulation of dispersion in convective atmospheric boundary layer with wind shear. *Atmospheric Environment* **26A**, 1561–1571.

Monin A. S. and Yaglom A. M. (1971) *Statistical Fluid Mechanics*, Vol. 1. MIT press, Cambridge.

Pasquill F. and Smith F. B. (1983) *Atmospheric diffusion.* Halsted Press, New York.

Peskin R. L. (1974) Numerical simulation of Lagrangian turbulent quantities in two and three dimensions. *Adv. Geophys.* **A18**, 141–163.

Philip J. R. (1967) Relation between Eulerian and Lagrangian statistics. *Boundary Layers Turbulence* (Physics of Fluids Supplement) 69.

Piomelli U. (1993) High Reynolds number calculations using the dynamic subgrid-scale stress model. *Phys. Fluid* **A5**, 1484–1490.

Riley J. J. and Patterson G. S. (1974) Diffusion experiments with numerically integrated isotropic turbulence. *Phys. Fluids* **17**, 292–297.

Saffman P. G. (1963) An approximate calculation of the Lagrangian autocorrelation coefficient for stationary homogeneous turbulence. *Appl. Sci. Res.* **11**, 245.

Sato Y. and Yamamoto, K. (1987) Lagrangian measurement of fluid particle motion in an isotropic turbulent field. *J. Fluid Mech.* **175**, 183–199.

Sawford B. L. (1982) Lagrangian Monte Carlo simulation of the turbulent motion of a pair of particles. *Q. J. R. Met. Soc.* **108**, 207–213.

Sawford B. L. (1984) The basis for, and some limitations of, the Langevin equation in atmospheric relative dispersion modelling. *Atmospheric Environment* **18**, 2405–2411.

Squires K. D. and Eaton, J. K. (1991) Lagrangian and Eulerian statistics obtained from direct numerical simulations of homogeneous turbulence. *Phys. Fluid* **A3**, 130–143.

Sykes R. I. and Henn D. S. (1992) Large-eddy simulation of concentration fluctuations in a dispersing plume. *Atmospheric Environment* **26A**, 3127–3144.

Taylor G. I. (1921) Diffusion by continuous movements. *Proc. Roy. Soc. Ser.* **A20**, 196–211.

Wei T. and Willmarth W. W. (1989) Reynolds number effects on the structure of a turbulent channel flow. *J. Fluid Mech.* **204**, 57–95.

Weil J. C. (1994) A hybrid Lagrangian dispersion model for elevated sources in the convective boundary layer. *Atmospheric Environment* **28**, 3433.

Wang Q., Squires K. D. and Wu X. (1994) Towards large eddy simulation of particle-laden turbulent shear flows. Report TM-3, Mechanical Engineering Department, University of Vermont, Burlington, VT 05405.

Wu X., Squires K. D. and Wang Q. (1995) On extension of the fractional step method to general curvilinear coordinate systems. *Numer. Heat Transfer* **27**, 175–194.

Yeung P. K. and Pope S. B. (1989) Lagrangian statistics from direct numerical simulation of isotropic turbulence. *J. Fluid Mech.* **207**, 531–586.

Zhang X. and Ghoniem A. F. (1993) A computational model for the rise and dispersion of wind-blown, buoyancy-driven plumes — I. Neutrally stratified atmosphere. *Atmospheric Environment* **27**, 2295.